Eur. Phys. J. B **61**, 47–58 (2008)
DOI: 10.1140/epjb/e2008-00026-0

THE EUROPEAN PHYSICAL JOURNAL B

Hydrodynamic interaction between two rotating tori

R.M. Thaokar[a]

Department of chemical engineering, Indian Institute of Technology, Bombay, Mumbai 400076, India

Received 13 August 2007 / Received in final form 29 November 2007
Published online 18 January 2008 –

Abstract. The hydrodynamic interactions between two rotating tori is studied. Two kinds of problems are addressed. The interaction between two force free tori is examined, for co and counter rotating cases, which should be relevant in the case of swimming of two toroidal animals and form the basis for interaction of a swarm of such swimmers, apart from the dynamics of a collection of stiff polymer rings. The second problem is the case of two non-translating rotating tori, a possible configuration in toroidal mixers for microfluidic devices. In the former case, analytical expression for translational velocity shows good agreement with the theory in the far field case and show a strong reduction in the velocities in the lubrication limit for the co-rotating case. The velocities are found to monotonically reduce to zero in the case of counter-rotating tori. For the latter case, the expression for velocity field is derived the net force acting on the torus is analytically calculated. The comparison with numerical results is encouraging both in the case of co as well as counter-rotation. The expressions derived for velocities should be useful in estimating pseudo-potentials between such pairs.

PACS. 47.85.Dh Hydrodynamics, hydraulics, hydrostatics

1 Introduction

Swimming at low Reynolds number has intrigued quite a few researchers and several models have been suggested in the last few decades to explain this interesting phenomenon [1–6]. The reversibility of Stokes equations permits only certain types of shape changes that are non-reciprocal and break the time-reversal symmetry. Only such sequence of configurations can make the animal move and most suggested models in the literature take this into account [4–6]. Purcell [3] in his famous article on life at low Reynolds number, suggests a rotating torus which can translate as a possible mechanism of motility of living organisms. The problem of a rotating torus is therefore important especially in understanding the movement of microorganisms and it would be interesting to examine the interactions between several such swimmers. The other instance where a rotating torus is encountered is the recently proposed nanomachine [7,8] which is a DNA mini-plasmid, set into rotations of the order of 1000 rad/s, by rectifying thermal fluctuations, using the ratchet effect. This DNA mini-plasmid can be looked upon as a rotating torus. The flow around a torus, rotating about its centerline, is now well understood [7–10]. A torus has coupled mobility (resistance) matrix, which results in translational propulsion on account of centerline rotation. The expression for mobility matrix was recently derived [7–9] and the magnitude of the velocity of a self-propelled, force free swimmer was calculated. The slender torus analysis was extended to "fat" tori, using the boundary integral method [9]. The method was also used to determine the propulsion velocity and "direction inversion" for the case of a torus moving along a cylindrical rod, threading through the "hole" in the torus [9].

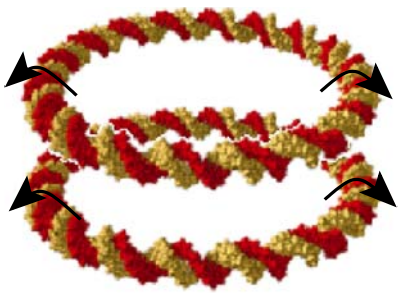

Fig. 1. Hydrodynamic interaction of two tori.

An issue of great interest in such systems is the interaction between two rotating tori (Fig. 1). If the tori are considered as models for biological organisms, the problem of interaction of two rotating tori would be important and can reveal the possibility of driven assembly leading to pattern formation in such systems [11], although multi-particle interactions are known to be different than two body interaction [12]. Recently, it was reported that two vortex rings can show chaos [13]. Although the flow over tori has been likened to flow due to vortex rings [14,15] in irrotational flows, there are differences arising from the

[a] e-mail: rochish@che.iitb.ac.in

fact that the torus has a definite rigid boundary, essentially at viscous Stokes flow conditions. There have been few investigations on hydrodynamic interactions between microorganisms, swimming at low Reynolds number. Analytical [16] and boundary integral methods [17,18] have been used in the past to investigate the interaction between two spheroidal bodies (bacteria) with rotating helical flagella. The computations, though, were limited to two cases: swimming side by side and swimming along one line. The minimum distance between the two spheroidal bodies was taken to be approximately equal to the minor axis of either spheroid, and lubrication effects were not addressed. More recently, there have been investigations [19] to derive hydrodynamic model for bacterial colonies suspended on agar plate. To model nutrient transfer and hydrodynamics, an ad-hoc interactive force between the microorganisms is often included, which in reality is unlikely to exist. Numerical hydrodynamic models have been used for two swimming organisms, the copepods for example, which are significantly larger than single-celled ciliates or flagellates, to calculate prey-encounter rates and other important quantities [20]. The behavior of such microorganisms is very different when they are close together, the analysis of which is mathematically difficult.

Recently, the hydrodynamic interaction of pairs of swimming cells was studied [21]. The cells were modeled as squirming sphere with prescribed tangential surface velocity. These are referred as squirmers by the authors on account of the mode of their motion. The center of mass of the sphere can be displaced from the geometric center, which is referred as bottom-heaviness. The interaction of two squirmers was calculated analytically for the limits of small (lubrication theory) and large separations (far field solution), and numerically using boundary-element method. A good match between analytical and numerical results was found for the translational-rotational velocities and for the stresslet of two squirmers. The principal results for two squirmers is that they first attract each other, a result of far-field interaction. However, at small separations, their orientation changes dramatically leading to separation.

The hydrodynamic interactions between two rotating tori is studied. The aim of this work is to derive interactions between two tori which can be used in the analysis of a collection of such tori. Two kind of problems are addressed: force free and non-translating tori. The interaction for force free motion of two tori should be relevant in the case of swimming of two toroidal animals and form basis for interaction of a swarm of such swimmers, as well as hydrodynamic interactions in dilute and semi-dilute polymeric solutions of semiflexible ring polymers.

The other problem is the case of two non-translating rotating tori, which should be pertinent in possible toroid like mixers in microfluidic devices. Analytical solutions for these two cases, in the slender torus and far field limit, are first derived for two configurations: co and counter-rotating tori. The results are then extended to non-slender tori and small separations (lubrication) using the boundary integral method.

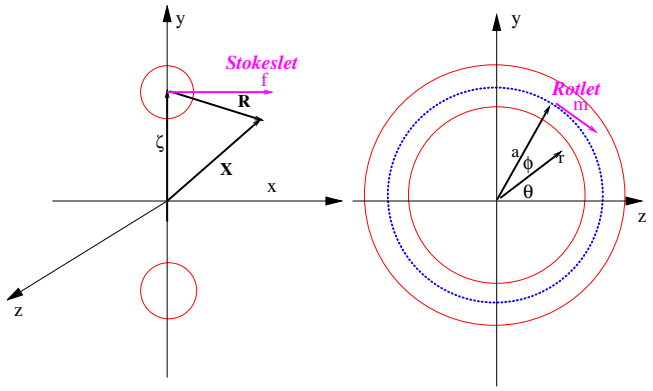

Fig. 2. Coordinate system for the torus: local representation in cylindrical coordinates for a single torus.

2 Analytical solution of a single rotating torus

Consider a torus with smaller diameter b and larger diameter a, rotating about its centerline with an angular velocity ω in a Newtonian fluid, in the zero Reynolds number limit (Fig. 2). In the analysis to follow, we indicate dimensional quantities by a tilde. The governing equations for the fluid are the Navier Stokes equations (continuity and momentum),

$$\tilde{\nabla} \cdot \tilde{\mathbf{u}} = 0 \tag{1}$$

$$\rho_f \left[\partial_{\tilde{t}} \tilde{\mathbf{u}} + \tilde{\mathbf{u}} \cdot \tilde{\nabla} \tilde{\mathbf{u}} \right] = -\tilde{\nabla} \tilde{p} + \mu \tilde{\nabla}^2 \tilde{\mathbf{u}} \tag{2}$$

where μ is the viscosity of the fluid. The physical quantities are non-dimensionalized as follows: the lengths are scaled by a, velocity with ωa, time by $1/\omega$, the stresses and the pressure by $\mu\omega$. With this non-dimensionalization the Navier Stokes equations are given by

$$\nabla \cdot \mathbf{u} = 0 \tag{3}$$

$$Re \left[\partial_t \mathbf{u} + \mathbf{u} \cdot \nabla \mathbf{u} \right] = -\nabla p + \nabla^2 \mathbf{u}, \tag{4}$$

where the Reynolds $Re = a^2 \rho_f / (\mu\omega)$. In this work, we consider the limit of low Reynolds number, so that the Navier Stokes equations reduce to the familiar Stokes equations

$$\nabla \cdot \mathbf{u} = 0 \tag{5}$$

$$-\nabla p + \nabla^2 \mathbf{u} = 0. \tag{6}$$

Here we use two coordinate systems (Fig. 2), the Cartesian $(\mathbf{e_x}, \mathbf{e_y}, \mathbf{e_z})$, and the cylindrical coordinate system $(\mathbf{e_x}, \mathbf{e_r}, \mathbf{e}_\theta)$. The unit vectors of the two coordinate systems are related by

$$\mathbf{e_y} = \mathbf{e_r} \cos\theta + \mathbf{e}_\theta \sin\theta \tag{7}$$

$$\mathbf{e_z} = \mathbf{e_r} \sin\theta - \mathbf{e}_\theta \cos\theta. \tag{8}$$

The solution for velocity can be expressed in terms of fundamental solutions of Stokes flow like the rotlet, the Stokeslet, the stresslet and the potential dipole [22,23].

For a rotating torus about its centerline, we assume a uniform distribution of rotlets of strength $m\mathbf{e_x} \times \mathbf{e_r}$ acting along the center line of the torus, m is a scalar and $\mathbf{e_x}$ is the unit vector in the direction of the axis of symmetry of the torus. $\mathbf{e_r}$ is the unit vector joining the center line with any point on the surface of torus and $\mathbf{e_x} \times \mathbf{e_r}$ is tangent to the circle at point $\zeta = a\mathbf{e_r}$ [10]. The dominant singularity representing the velocity field of a "self propelled rotating torus" is expected to be the rotlet. The effect of the Stokeslet (force singularity) and the potential dipole (a higher order singularity) is considered later. The velocity in terms of the rotlet is then given by

$$\mathbf{u} = m\frac{\mathbf{e_x} \times \zeta \times \mathbf{R}}{R^3}. \tag{9}$$

Any reference point in the fluid, can be represented in cartesian coordinates (denoted with $()^c$) by $\mathbf{X} = (x, r\cos\theta, r\sin\theta)^c$, while the centerline of the torus is given by $\tilde{\zeta} = (0, a\cos\phi, a\sin\phi)^c$. Here, θ is the azimuthal angle in the cylindrical coordinate system for any reference point X in the fluid, while ϕ defines the azimuthal angle subtended by the point rotlet ζ, acting along the centerline. Choosing the unit-length a, the vector joining the reference point and the centerline becomes $\mathbf{R} = \mathbf{X} - \zeta = (x, \sqrt{r^2+1-2r\cos(\phi-\theta)}, \phi-\theta)^{cyl}$ with $(...)^{cyl}$ denoting the the cylindrical coordinates with magnitude R given by $\sqrt{r^2+x^2+1-2r\cos(\phi-\theta)}$. The velocity at point $\mathbf{X}$ generated by the distribution of the point rotlets acting along the centerline can be obtained by integrating over ϕ. The velocity components are

$$u_x = \int_0^{2\pi} d\phi \left[m\frac{a - r\cos(\phi-\theta)}{R^3} \right] \tag{10}$$

$$u_r = \int_0^{2\pi} d\phi \left[mx\frac{\cos(\phi-\theta)}{R^3} \right] \tag{11}$$

$$u_\theta = \int_0^{2\pi} d\phi \left[mx\frac{\sin(\phi-\theta)}{R^3} \right]. \tag{12}$$

Since the rotlet is a special case of the fundamental solution which is identically annihilated by the Laplacian $\nabla^2\mathbf{u} = 0$, the pressure due to the rotlet (Eq. (6)) is a constant.

The angular component of the velocity is zero by symmetry. The velocities in equations (10) and (11) can be integrated and easily expressed in terms of complete elliptic integrals $E(k)$ and $K(k)$ (Appendix A), where k is defined as, $k^2 = 4r/\left[x^2 + (r+1)^2\right]$.

The velocities in terms of these elliptic functions are given by (Appendix A),

$$u_x = \frac{m(I_3 - rI_4)}{C^3} \tag{13}$$
$$u_r = \frac{mxI_4}{C^3}$$

with $C = \sqrt{x^2+(r+1)^2}$ and I_3 and I_4 elliptic integrals given in Appendix A.

In our analysis we also consider external forces acting on the torus, and analyze two additional singularities, the potential dipole of strength d_{px} and the Stokeslet of strength f_x in the x direction. The velocity due to a ring of point forces and point dipoles, distributed along the centerline is now discussed. Consider the velocity due to a Stokeslet of strength f which is given by

$$\mathbf{u} = \left(\frac{\mathbf{I}}{R} + \frac{\mathbf{RR}}{R^3} \right) \cdot \mathbf{f}. \tag{14}$$

Here $\mathbf{RR}$ denotes the dyadic product, $\mathbf{I}$ is the identity matrix and $\mathbf{f}$ is a point force vector. The pressure due to a Stokeslet is given by

$$p = \frac{2\mathbf{R}\cdot\mathbf{f}}{R^3}. \tag{15}$$

An axially symmetric situation is considered here, i.e. a Stokeslet acting in the flow direction, x, and of constant magnitude f so that $\mathbf{f} = f_x\mathbf{e_x}$. The velocity is then given by

$$\mathbf{u} = \left(\frac{\mathbf{e_x}}{R} + \frac{\mathbf{R}x}{R^3} \right) f_x. \tag{16}$$

Similarly as in the rotlet case , using $\mathbf{R} = \mathbf{X} - \zeta$ with magnitude $R = \sqrt{x^2+(r+1)^2 - 4r\cos^2(\phi/2)}$, and integrating over the ϕ distribution of the ring of point Stokeslet, we obtain

$$u_x = f\int_0^{2\pi} d\phi \left[\frac{1}{R} + \frac{x^2}{R^3} \right] = f_x\left(\frac{I_1}{C} + x^2\frac{I_3}{C^3} \right) \tag{17}$$

$$u_r = fx\int_0^{2\pi} d\phi \left[\frac{r}{R^3} - \frac{\cos(\phi-\theta)}{R^3} \right] = \frac{xf_x(rI_3 - I_4)}{C^3} \tag{18}$$

$$p = 2fx\int_0^{2\pi} d\phi \left[\frac{\cos(\phi-\theta)}{R^3} \right] = \frac{2xf_xI_3}{C^3}. \tag{19}$$

It is known that the Stokeslet and its higher derivatives are solutions to Stokes equations [23]. Thus if $\mathbf{G}$ represents a Stokeslet then $\nabla^2\mathbf{G}$ is also a solution to the Stokes equation and is called as the potential dipole. The velocity due to a potential dipole can be easily derived as

$$\mathbf{u} = \left(\frac{\mathbf{I}}{R^3} - \frac{\mathbf{3RR}}{R^5} \right) \cdot \mathbf{d}. \tag{20}$$

Consider the distribution of potential dipoles along a ring, acting in the x direction, such that $\mathbf{d} = d_{px}\mathbf{e_x}$, the x and the r directional velocities are given by,

$$u_x = d_{px}\int_0^{2\pi} d\phi \left[\frac{1}{R^3} - \frac{3x^2}{R^5} \right] = f_x\left(\frac{I_3}{C^3} - \frac{3x^2I_6}{C^5} \right) \tag{21}$$

$$u_r = 3xd_{px}\int_0^{2\pi} d\phi \left[-\frac{r}{R^5} + \frac{\cos(\phi-\theta)}{R^5} \right] = -\frac{3d_{px}x(rI_6 - aI_7)}{C^5}. \tag{22}$$

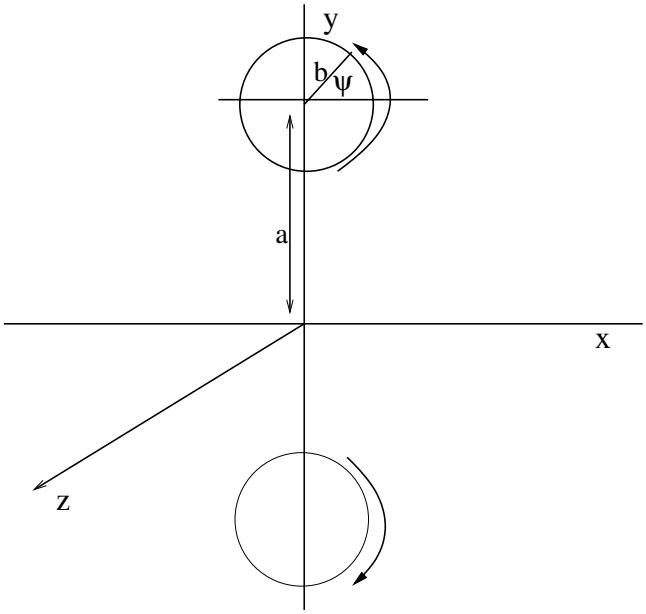

Fig. 3. Local parameterization of the torus.

Note that there is no pressure contribution of the potential dipole [23]. The net velocity can be written as

$$u_x = \frac{m}{C^3}(I_3 - rI_4) + d_{px}\left(\frac{I_3}{C^3} - 3x^2\frac{I_6}{C^5}\right) + f_x\left(\frac{I_1}{C} + x^2\frac{I_3}{C^3}\right) \quad (23)$$

$$u_r = \frac{mxI_4}{C^3} - \frac{3d_{px}x}{C^5}(rI_6 - I_7) + \frac{xf_x}{C^3}(rI_3 - I_4)$$

$$p = \frac{2f_x x I_3}{C^3} \quad (24)$$

where p is the pressure and has contribution only from the Stokeslet. For a torus rotating with angular velocity ω and translating with velocity U_x the boundary conditions are $\tilde{u}_x = \omega(a - \tilde{r}) + \tilde{U}_x$ and $\tilde{u}_r = \omega\tilde{x}$ at the surface of the torus. The non-dimensional boundary conditions thus become $u_x = (1 - r) + U_x$ and $u_r = x$. In the special case of an immobile torus, we set $U_x = 0$. Further, the case of a slender torus (the ratio of the two radii of the torus, $\epsilon = b/a$ is small) is considered here, and the surface is locally parameterized by an angle ψ, such that $x = \cos\psi$ and $r = 1 + \epsilon\sin\psi$ (Fig. 3). This implies the expansion $k^2 = 1 - \frac{\epsilon^2}{4} + O(\epsilon)^3$ in the slender torus limit. The asymptotic expressions for the elliptic integrals in the $k = 1$ limit (Appendix A) can therefore be used to simplify the expressions. The boundary conditions demand a scaling , $m = m_0\,\epsilon^2$, $d_{px} = \epsilon^4 d_{px0}$ and $f_x = \epsilon^2 f_{x0}$. The boundary conditions are x and r directional no slip velocity conditions respectively.

$$U_x - \epsilon\sin\psi = -2\,\epsilon m_o\sin\psi - \frac{\epsilon^2(m_o + 4d_{pxo} - 2f_{xo})}{2}\cos 2\psi + \frac{\epsilon^2}{2}\left(2m_o\left(\log\frac{8}{\epsilon} - \frac{1}{2}\right) + 4f_{xo}\left(\log\frac{8}{\epsilon} + \frac{1}{2}\right)\right) \quad (25)$$

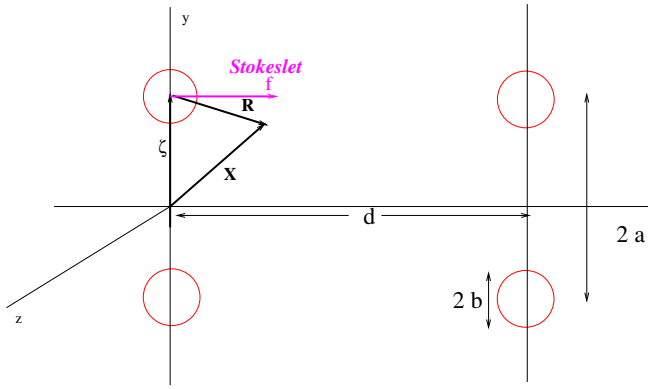

Fig. 4. Coordinate system for interaction of two torus.

$$\epsilon\cos\psi = 2\,\epsilon m_o\cos\psi - \frac{\epsilon^2(m_o + 4d_{pxo} - 2f_{xo})}{2}\sin 2\psi. \quad (26)$$

At $O(\epsilon)$, we get the strength of the rotlet as $m_o = \frac{1}{2}$ which is the central result of [10].

Equations (25) and (26) can be solved in two situations: a force free torus and a stationary torus and these are discussed in the Appendix B.

3 Hydrodynamic interaction between two tori

Consider the hydrodynamic interaction of two tori (Fig. 4) separated axially by a distance d. To calculate the interaction, it is necessary to specify either the force and torque on the surface of the torus (the mobility problem) and calculate the velocities of the two tori. Alternatively, one can prescribe the translational and angular velocity of the two tori (resistance problem) and calculate the additional force and torque required to maintain those velocities as a result of hydrodynamic interaction.

3.1 Force-free tori

The "mobility problem" which is relevant in hydrodynamic interaction in a collection of self-propelled animals is first addressed. The two tori remain force free in the x direction, but are allowed to move with a constant angular velocity ω. The additional torque exerted is absorbed by the tori. The free draining velocity of the rotating tori can then be given by the imposed velocity of the second torus acting on the first torus and vice versa. In addition to this the tori travel at their own self propelled velocity given by the expression (53). Consider the first torus, whose velocity is given by equation (23). This becomes the ambient velocity field for the second torus, such that,

$$u_x^\infty = \frac{m}{C^3}(I_3 - rI_4) + d_p^x\left(\frac{I_3}{C^3} - 3x^2\frac{I_6}{C^5}\right) \quad (27)$$

$$u_r^\infty = \frac{mxI_4}{C^3} - \frac{3d_p^x x}{C^5}(rI_6 - I_7) \quad (28)$$

is evaluated at $\tilde{x} = d + a\cos\psi$ and $\tilde{r} = a + b\sin\psi$, which correspond to the non-dimensional positions, $x = \delta + \cos\psi$, and $r = 1 + \epsilon\sin\psi$. Here the non-dimensional separation between the two tori is given by $\delta = d/a$. This in the far field limit $\delta \to \infty$, means k is $O(1/\delta)^2$ and the asymptotic expressions for the elliptic integrals around $k = 0$ can now be used (Appendix A). Substituting $m_o = 1/2$ and $d_{pxo} = -1/8$, corresponding to the solution for a single force free torus, the velocity at the center of the torus is given by $x \to \delta$ and $r \to 1$

$$u_{x\infty} = \pi\epsilon^2\left(\frac{(11+2\delta^2)}{2(4+\delta^2)^{5/2}}\right) \tag{29}$$

$$u_{r\infty} = \pi\epsilon^2\left(\frac{2\pi\epsilon^2(15+2\delta^2)}{4\delta(4+\delta^2)^{5/2}}\right). \tag{30}$$

In the far field limit, the net translational velocity of the tori is therefore given by,

$$U_x = \frac{\epsilon^2}{2}\left(\log\frac{8}{\epsilon} - \frac{1}{2}\right) \pm \pi\epsilon^2\left(\frac{(11+2\delta^2)}{2(4+\delta^2)^{5/2}}\right) \tag{31}$$

for co and counter-rotating tori respectively.

3.2 Non-translating tori

3.2.1 Force acting on the tori

We now consider the resistance problem. The expression for the velocity of a non-translating rotating torus is dervied in the Appendix B and is given by

$$u_x = \frac{m}{C^3}(I_3 - rI_4) + d_{px}\left(\frac{I_3}{C^3} - 3x^2\frac{I_6}{C^5}\right) + f_x\left(\frac{I_1}{C} + x^2\frac{I_3}{C^3}\right) \tag{32}$$

$$u_r = \frac{mxI_4}{C^3} - \frac{3d_{px}x}{C^5}(rI_6 - I_7) + \frac{xf_x}{C^3}(rI_3 - I_4) \tag{33}$$

involving a rotlet, a dipole and a Stokeslet. The solution for a non-translating, rotating, single torus is given by,

$$m_0 = \frac{1}{2}$$
$$f_{xo} = -\frac{\epsilon^2}{4}\left[\frac{\ln(8/\epsilon) - 1/2}{\ln(8/\epsilon) + 1/2}\right]$$
$$d_{pxo} = -\frac{1}{4}\frac{\log\frac{8}{\epsilon}}{\log\frac{8}{\epsilon} + \frac{1}{2}}. \tag{34}$$

The hydrodynamic interaction of two such tori , rotating and not translating, can be calculated in the far field approximation to the lowest order as follows: at the zeroth order, the velocities of the two tori are the expression 32, 33. The first order hydrodynamic interaction can be obtained by requiring that the reflected fields satisfy no-slip condition. This leads to estimation of the force exerted on a torus which is immersed in the velocity u_∞ produced by the rotation of the other torus. Therefore, if we consider the first torus, whose velocity is given by equations (32) and (33). This becomes the ambient velocity field for the second torus, evaluated at $\tilde{x} = d + a\cos\psi$ and $\tilde{r} = a + b\sin\psi$, which correspond to the non-dimensional positions, $x = \delta + \cos\psi$, and $r = 1 + \epsilon\sin\psi$. Here the non-dimensional separation between the two tori is $\delta = d/a$. This in the far field limit $\delta \to \infty$, means k is $O(1/\delta)^2$ and the asymptotic expressions for the elliptic integrals around $k = 0$ can now be used (Appendix A).

The x directional velocity at the center of the torus in the $x \to \delta$ and $r \to 1$ limit is,

$$u_{x\infty} = \frac{\pi\epsilon^2}{4}\left(\frac{89 + 36\delta^2 + 4\delta^4 - 2(45 + 4\delta^2(7+\delta^2))\log\frac{8}{\epsilon}}{(4+\delta^2)^{5/2}(1 + 2\log\frac{8}{\epsilon})}\right) \tag{35}$$

and the non-dimensional force on the torus is given by

$$F = 4\pi^2\epsilon^2\frac{(\log 8/\epsilon - 1/2)}{(\log 8/\epsilon + 1/2)} \mp 8\pi^2\frac{u_{x\infty}}{(\log 8/\epsilon + 1/2)}. \tag{36}$$

The first term in equation (36) is the force required to keep a rotating torus stationary. The second term is the additional force due to hydrodynamic interaction in the co and counter-rotating case.

3.2.2 Velocity field for two non-translating tori

We now seek the velocity profile at any point in the fluid for a system of two tori non-translating and rotating in co or counterwise fashion. The disturbance velocity which we indicate by a *tilde* is assumed to consist of a distribution of rotlet, stresslet and potential dipoles along the center line in both x and the r direction.

The velocity field is then given by

$$\tilde{u}_i = \tilde{f}_j G_{ij} + \tilde{d}_j D_{ij} + \tilde{t}_j R_{ij} + S_{jk}\Psi_{ijk} \tag{37}$$

where the fundamental solutions have following definitions:

$$G_{ij} = \frac{\delta_{ij}}{R} + \frac{x_i x_j}{R^3} \tag{38}$$
$$D_{ij} = \frac{\delta_{ij}}{R} - \frac{3x_i x_j}{R^3}$$
$$\Psi_{ijk} = \frac{x_i\delta_{jk}}{R^3} - \frac{3x_i x_j x_k}{R^5}R_{ij}.$$

R_{ij} is a rotlet as defined earlier. With $\tilde{\mathbf{f}} = f_x\,\mathbf{e_x} + f_r\cos\phi\,\mathbf{e_y} + f_r\sin\phi\,\mathbf{e_z}$, $\tilde{\mathbf{d}} = d_x\,\mathbf{e_x} + d_r\cos\phi\,\mathbf{e_y} + d_r\sin\phi\,\mathbf{e_z}$ represent the Stokeslet and dipole strength. The rotlet is constructed in the same manner as for the case of a single torus, and the stresslet strength is defined as:

$$\begin{pmatrix} s_{xx} & s_{xr}\cos\theta & s_{xr}\sin\theta \\ s_{xr}\cos\theta & s_{rr}\cos^2\theta & s_{rr}\sin\theta\cos\theta \\ s_{xr}\sin\theta & s_{rr}\sin\theta\cos\theta & s_{rr}\sin^2\theta \end{pmatrix}.$$

Incompressibility demands that $s_{rr} = -s_{xx}$ and the stresslet is therefore symmetric traceless. The velocity can then be written as follows:

$$\begin{aligned} u_x = {} & \frac{m}{C^3}(I_3 - rI_4) + \tilde{f}^x\left(\frac{I_1}{C} + x^2\frac{I_3}{C^3}\right) \\ & + \tilde{d}^x\left(\frac{I_3}{C^3} - 3x^2\frac{I_6}{C^5}\right) + \frac{\tilde{f}^r}{C^5}(-I_3 + rI_4) \\ & - \frac{\tilde{d}^r 3x}{C^5}(-I_6 + rI_7) + \frac{1}{C^5}\left(3xs_{xr}(xI_6 - rxI_7)\right) \\ & + \frac{1}{C^5}\left(3xs_{xx}(I_6 - 2rI_7 - x^2I_6 + r^2I_8)\right) \end{aligned} \tag{39}$$

$$\begin{aligned} u_r = {} & \frac{mxI_4}{C^3} + \frac{\tilde{f}^x}{C^3}(rI_3 - I_4) - \frac{\tilde{d}^x 3x}{C^5}(rI_6 - I_7) \\ & + \tilde{f}^r\left(\frac{I_2}{C} - \frac{rI_3 - rI_5 + (r^2+1)I_4}{C^3}\right) \\ & + \tilde{d}^r\left(\frac{I_4}{C} + \frac{3rI_6 - 3(r^2+1)I_7 + 3rI_8}{C^5}\right) \\ & - 3s_{xr}\left(\frac{((x + r^2x)I_3 - rx)}{C^3} - rx\frac{I_2}{C}\right) \\ & - \frac{3s_{xx}}{C^5}(I_7 - rI_6 - 2rI_8 + r^2I_9 - r^3I_8 + rx^2I_6 \\ & + (2r^2 - x^2)I_7). \end{aligned} \tag{40}$$

In the above expressions, the elliptic integrals are evaluated using the asymptotic expansion around $k = 1$, given in the Appendix A.

The strength of the rotlet, Stokeslet and dipole are obtained by applying the boundary conditions on the surface of the torus, that is at $x = \cos\theta, r = 1 + \epsilon\sin\theta$, such that,

$$-\tilde{u}_i^\infty = \tilde{u}_i \tag{41}$$

$$-\int_0^{2\pi} d\theta(\mathbf{x} \times \tilde{u}_i^\infty) = \int_0^{2\pi} d\theta(\mathbf{x} \times \tilde{u}_i). \tag{42}$$

The boundary condition (41) gives the strength of the Stokeslet and the potential dipole in the two directions x and r. The boundary condition (42) gives the strength of the rotlet. The value of the stresslet is obtained by taking the dyadic product of the velocity with the lever arm, and equating the symmetric part of the corresponding matrix.

$$-\int_0^{2\pi} d\theta(x_i\tilde{u}_j^\infty) = \int_0^{2\pi} d\theta(x_i\tilde{u}_j) \tag{43}$$

The expression for the strengths of different singularities is calculated as:

$$\begin{aligned} \tilde{f}^x &= \frac{\pi(1 - 2\log\frac{8}{\epsilon})}{\delta(1 + 2\log\frac{8}{\epsilon})^2} \\ \tilde{f}^r &= \frac{\pi(1 - 2\log\frac{8}{\epsilon})}{2\delta^2(-5 + 2\log\frac{8}{\epsilon})(1 + 2\log\frac{8}{\epsilon})} \\ \tilde{m} &= -\frac{\pi(-4 + 6\log\frac{8}{\epsilon} + 4\log 8\log\frac{8}{\epsilon^2} + 4(\log\epsilon)^2}{4\delta(1 + 2\log\frac{8}{\epsilon})^2}) \\ \tilde{s}_{xxo} &= \frac{\pi}{24\delta^2}\left(15 + \frac{4}{-5 + 2\log\frac{8}{\epsilon}} - \frac{28}{1 + 2\log\frac{8}{\epsilon}}\right) \\ \tilde{s}_{ppo} &= -\pi\frac{1 - 72(\log 2)^2 + \log 64 + 2(-1 + 4\log\frac{64}{\epsilon})\log\epsilon}{2\delta(1 + 2\log\frac{8}{\epsilon})^2} \end{aligned} \tag{44}$$

with the dipole strengths given by

$$\begin{aligned} \tilde{d}^x &= \frac{b^2}{2}\tilde{f}^x, \\ \tilde{d}^r &= \frac{b^2}{2}\tilde{f}^r. \end{aligned} \tag{45}$$

4 The boundary integral method

The results in the slender limit are practically useful, especially, in the case of polymer rings and miniplasmids. It would, however, be interesting to extend the results to the case in which the torus thickness is of the same order as the internal radius. For the motion of such a non-slender torus it is necessary to revert to some kind of numerical method. Here we use the boundary integral method which is a singularity method and is best suited to solve Stokes equations. The drag calculation (resistance problem) involves solving integral equation of the first kind, which are known to generate ill conditioned matrices [22], although converged non-oscillatory solutions are reported in certain specific cases [24]. For force calculation in the torus, we do get well behaved converged solutions which are in good agreement with the analytical solution in the slender torus limit. The calculations are then extended to the non-slender limit. In fact, the analytical expressions reported in Section 4 are multipole expansions of the complete integral equation, for force distribution, which can be solved numerically using the boundary integral method [23]. Note that multipole expansions are different moments of the Stokeslet about the centerline of the torus [23].

The representation of the velocity by the boundary integral equation can be written as

$$\begin{aligned} u_i(\mathbf{x}_0) = {} & -\frac{1}{8\pi\mu}\int dS(\mathbf{x})G_{ij}(\mathbf{x},\mathbf{x}_0) \\ & + \frac{1}{8\pi}\int dS(\mathbf{x})u_j(\mathbf{x})T_{ijk}(\mathbf{x},\mathbf{x}_0)n_k(\mathbf{x}) \end{aligned} \tag{46}$$

where $G_{ij}(\mathbf{x},\mathbf{x}_0) = \left(\frac{\delta_{ij}}{r} + \frac{\mathbf{x}_i\mathbf{x}_j}{r^3}\right)$and $T_{ijk}(\mathbf{x},\mathbf{x}_0) = \frac{x_ix_jx_k}{r^5}$ where $r = |\mathbf{x} - \mathbf{x}_0|$, S(x) is the surface area of the two bodies (tori) over which integration is carried out and n_k is

the local unit outward normal to the surface. The equation is derived in Appendix C [9,22]. We make use of the axisymmetry in the problem, akin to the analytical solution discussed in the earlier section. The Greens functions are modified after integration in the azimuthal direction and are provided in several references [22,23]. These are expressed in terms of elliptic integrals of the first and second kind. In the above equation $u_i(\mathbf{x})$ is known and is given by $(U_x + (1-r), x)$. The integrals are solved by discretizing the arc length into numerous elements and interpolating using cubic splines. The Greens function exhibit $-\log r$ singularity as $r \to 0$ that is $\mathbf{x} \to \mathbf{x}_0$. The singularity is handled in the usual way [22] by subtracting the singular part from the Greens functions and carefully integrating it analytically. The force, velocity, arc length and all other variables are also expressed as cubic splines. The condition of no net x directional force (force free torus) is enforced to get the unknown longitudinal translational velocity for both the tori. The comparison of the asymptotic and numerical solutions are discussed in the following section. In far field simulations reported in this work, we have used 80 elements for discretization. In the lubrication limit, the number of elements was increased to as high as 400. In all the cases, the results were confirmed by doubling the number of elements and the tolerance was set at less than 0.1%. The code was also confirmed with analytical results in the far-field limit as well as by ensuring that Stokes reversibility namely, *zero* relative velocity in the case of co-rotating tori and equal and opposite absolute velocity in the case of counter-rotating tori is obeyed. In the non-translating case the theoretical expectation of equal force on the two tori was confirmed through simulations.

5 Results and discussion

The interaction between two co and counter-rotating tori is studied for two cases: force-free and non-translating tori. Analytical solutions are derived using singularity method as discussed in Section 3 and the boundary integral method was used to extrapolate beyond the analytical limits.

5.1 Force-free tori

Tori are the best prototypes for self propelled particles and the interaction is important in understanding processes like bio-convection in such systems. We consider here, the interaction between two co and counter- rotating tori which are force free and self propelled. This is valid especially for low Reynolds number swimmers, as also for the hydrodynamic interaction between stiff polymer rings [9]. The analytical expressions for the case of co and counter-rotating tori are given by 31. In the boundary integral method for this case, the net force of the two tori is independently set to zero to determine the unknown translational velocities. The magnitude of translational velocity is found to be the same for the two tori. Infact, this was used to check the accuracy of the numerical method.

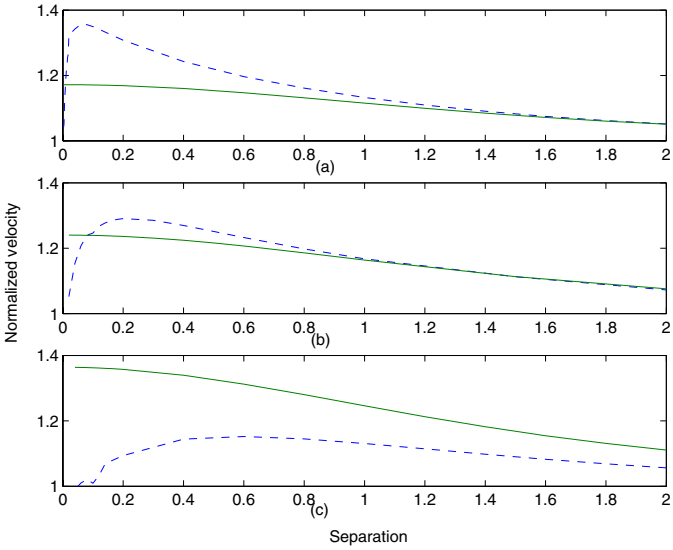

Fig. 5. Comparison of the analytical (—) and numerical (----) results for non-dimensional translational velocity versus separation for co-rotating tori (a) $\epsilon = 0.01$, (b) $\epsilon = 0.05$ and (c) $\epsilon = 0.25$.

While the relative velocity is zero for the co-rotating case, it is twice the absolute velocity in the case of counter-rotating tori.

5.1.1 Co-rotating tori

Figure 5 shows the comparison between the analytical and numerical non-dimensional velocity $U = \frac{U^*}{U_t}$ where $U_t = \frac{\epsilon^2}{2}(\log\frac{8}{\epsilon} - \frac{1}{2})$, with the non-dimensional separation $\delta = \tilde{d}/a$. U_t is the non-dimensional free-stream velocity of a single torus rotating with angular velocity ω. The figure illustrates that the comparison between the analytical and the numerical results is fairly good for separation as low as $\delta = 1$, especially for the case of slender tori with $\epsilon = 0.01, 0.05$. The deviation for $\epsilon = 0.25$ though, is substantial. Figure 6 shows the comparison between the normalized translational velocities of the tori for three slenderness ratios. In the far field $\delta \to \infty$, the normalized velocity $U \to 1$, since the velocity is normalized by U_t. It is seen that the translational velocity increases as the separation decreases, in accordance with the theory, and with a value larger than unity indicating reinforcement of velocity (Fig. 8a). However, at small separations, a sharp fall in the absolute velocity is observed. The descent is more dramatic for slender tori. The velocities scale logrithmically in the lubrication limit (Fig. 7). In all the simulations carried out, the Stokes law reversibility is obeyed and the relative velocity of the two tori is zero. The sharp reduction in the absolute velocity is an indication of "slow down" of the tori, and disappearance of hydrodynamic interaction, an effect which is observed in the case of counter-rotating tori as well, and a result of strong non-linearity. Since the torus slenderness ϵ, the non- dimensional thickness of the torus, is the only length scale relevant in this case, we find

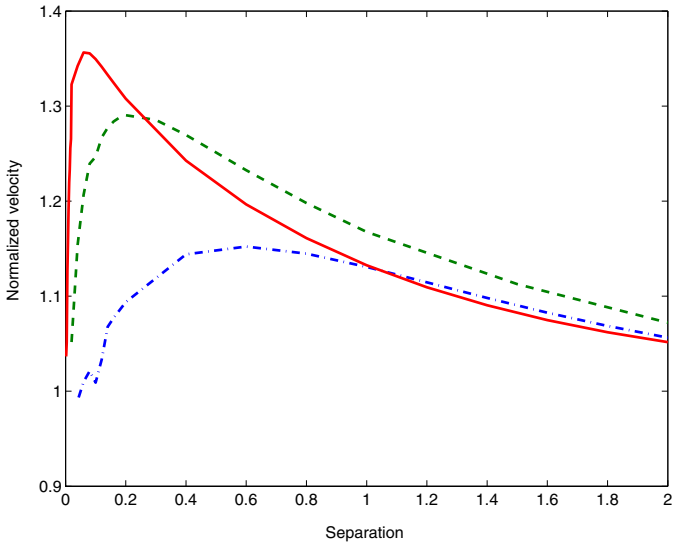

Fig. 6. Comparison of the numerical results for non-dimensional translational velocity versus separation for co-rotating tori (— $\epsilon = 0.01$, - - - - $\epsilon = 0.05$, —·—· $\epsilon = 0.25$).

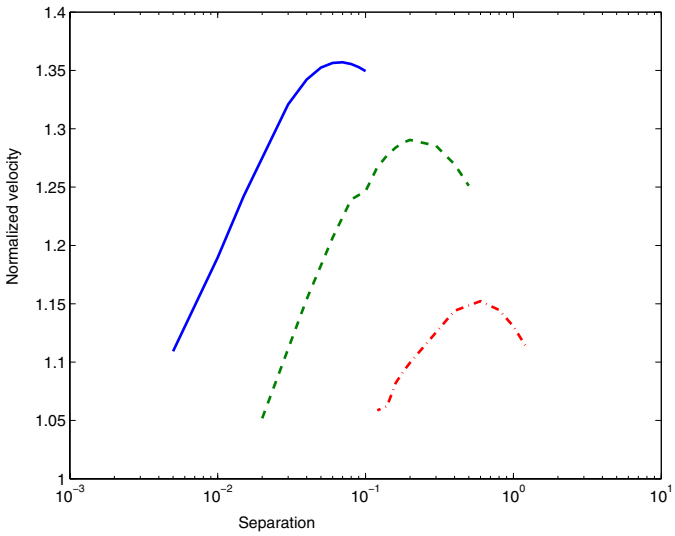

Fig. 7. Comparison of the numerical results for non-dimensional translational velocity versus separation for co-rotating tori in the lubrication limit (— $\epsilon = 0.01$, - - - - $\epsilon = 0.05$, —·—· $\epsilon = 0.25$).

that the sharp decrease in the velocity in the co-rotating case occurs at separations of the same orders as the torus diameter.

5.1.2 Counter-rotating tori

The relative velocity of two counter-rotating tori is non-zero, infact it is equal to twice the absolute velocity of each of the tori. Figure 9 shows the variation of the velocity of the tori with separation for three different slenderness ratios. The agreement between the numerical and the analytical results improves with the slenderness ratio ϵ. The reason for the drop in the velocity for counter-rotating tori

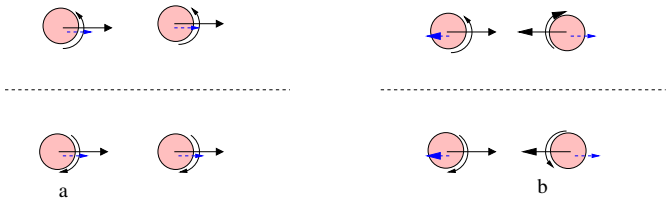

Fig. 8. Schematics of reinforcement and annihilation of velocities in the co and counter rotating cases: solid arrow is for the single torus velocity while the dashed arrow indicates correction

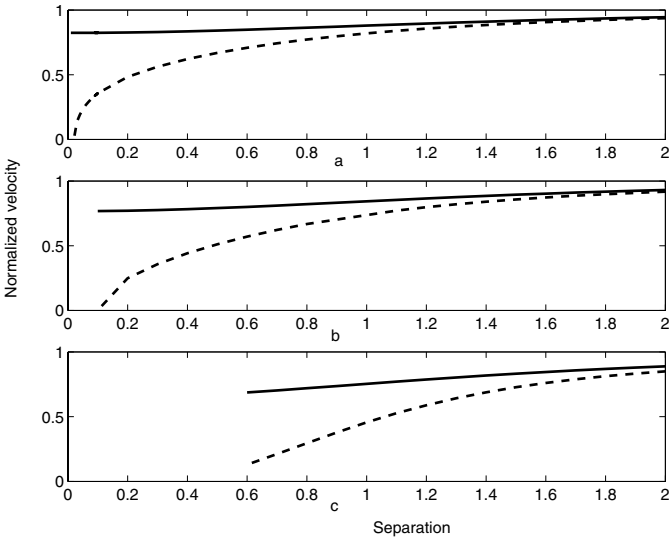

Fig. 9. Comparison of the analytical (—) and numerical (· · ·) results for non-dimensional translational velocity versus separation for counter-rotating tori (a) $\epsilon = 0.01$, (b) $\epsilon = 0.05$ and (c) $\epsilon = 0.25$.

can be understood from Figure 8b. Figure 10 shows the numerical results for the variation of translational velocity as a function of the separation. The velocity approaches zero at non-zero separations and hints at possible slowdown and aggregation in a collection of tori. The drastic slowdown can be attributed to strong lubrication and nonlinear interaction.

5.2 Interaction between stationary tori

Non-translatory, rotating tori can be potentially used in microfluidic devices for pumping fluids. They may also be encountered in constrained polymer dynamics of miniplasmids and stiff rings. The analytical expression for the force in the case of co and counter-rotating tori is given by equation (36). In the boundary integral method for this case, the net force is directly calculated by the solving the integral equation (46) and imposing the rotational velocity on the surface. The translational velocity is maintained at zero. The magnitude of the x directional force is equal in magnitude for the two tori. This was used to check the accuracy of the numerical method. While the force is equal and opposite for the co-rotating case, it is equal and in the same direction for the case of counter-rotating tori.

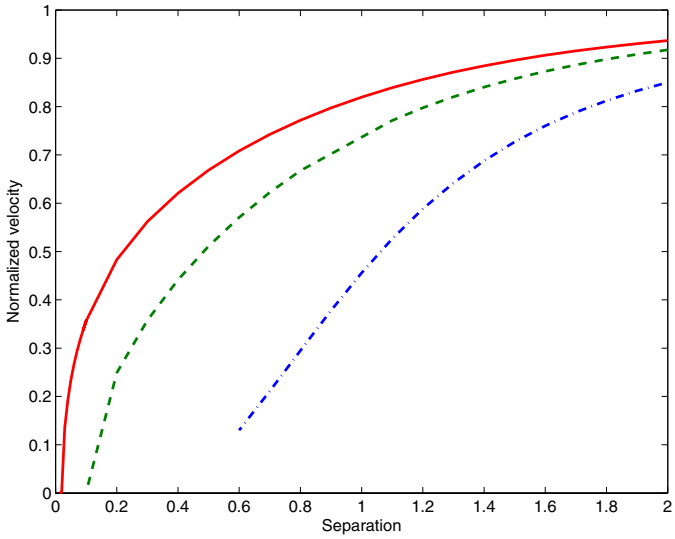

Fig. 10. Comparison of the numerical results for non-dimensional translational velocity versus separation for counter-rotating tori (— $\epsilon = 0.01$, ---- $\epsilon = 0.05$, —·— $\epsilon = 0.25$).

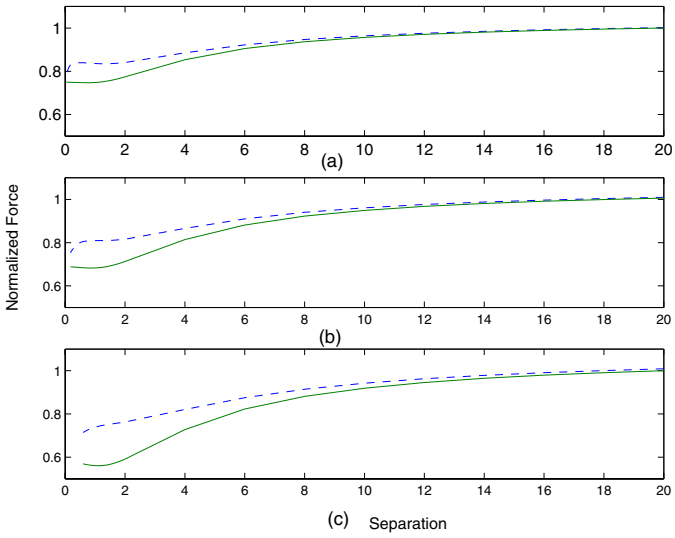

Fig. 11. Comparison of the analytical (—) and numerical (----) results for non-dimensional force versus separation for co-rotating tori (a) $\epsilon = 0.01$, (b) $\epsilon = 0.05$ and (c) $\epsilon = 0.25$.

5.2.1 Co-rotating tori

Figure 11 shows the variation of the total force acting upon the tori with separation in the case of co-rotating configuration. The total normalized force shows close match with analytical theory for separations of the order of $\delta = 10$ for all the three slenderness ratios, although the agreement improves considerably with decreasing ϵ. This can be compared with the force free case in which the analytical and numerical results agree reasonably at separations as low as $\delta = 2$. In general, the good agreement between the analytical and the numerical results can be attributed to the $O(\epsilon^2)$ variation of both the mean and the perturbation quantities.

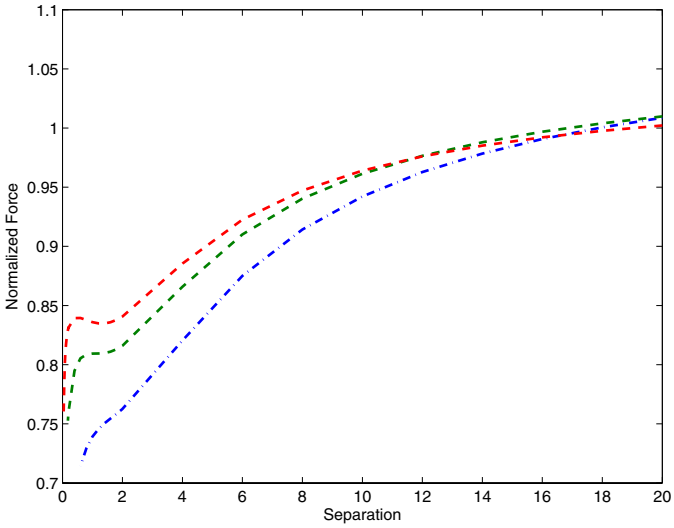

Fig. 12. Comparison of the numerical results for non-dimensional force versus separation for co-rotating tori in the lubrication limit (— $\epsilon = 0.01$, ---- $\epsilon = 0.05$, —·— $\epsilon = 0.25$).

The force acting on the two tori is equal, and lesser than that acting on the tori in the absence of the other. This can be attributed to the opposite direction of force in this configuration, resulting in the value of normalized force being less than unity. The numerical values of the normalized force is shown in Figure 12 for three different slenderness ratios and a qualitative change in the nature of the curve is observed at larger values of ϵ, especially at small separations. Interestingly, it is observed that there is a finite force even at very low separations and that the hydrodynamic interactions never really cancel each other.

5.2.2 Counter-rotating tori

For the case of counter-rotating tori, a similar behavior is observed (Fig. 13). The force on the tori increases with decrease in separation, since the force on a single torus and the force because of hydrodynamic interaction act in the same direction. The numerical and analytical values are found to match for even smaller values of separation than the co-rotating cases (Fig. 13). Figure 14 shows the variation of force (numerical) with separation and the divergence in force with slenderness ratio, is found to be larger than the co-rotating case, especially at small separations. The results obtained in the co and the counter-rotating cases can be easily explained from the schematics (Fig. 15).

It should be mentioned that although the present work deals with axi-symmetric interaction between tori, non-axisymmetry can have dramatic effects on the system. In-fact, the recent work by Pedley on squrimers [11] consider three dimensional orientation of the squirmers and find interesting near and far field dynamics that include attraction and change of orientation.

In the non-axisymmetric case, the velocity field experienced by a swimmer on account of the motion of another

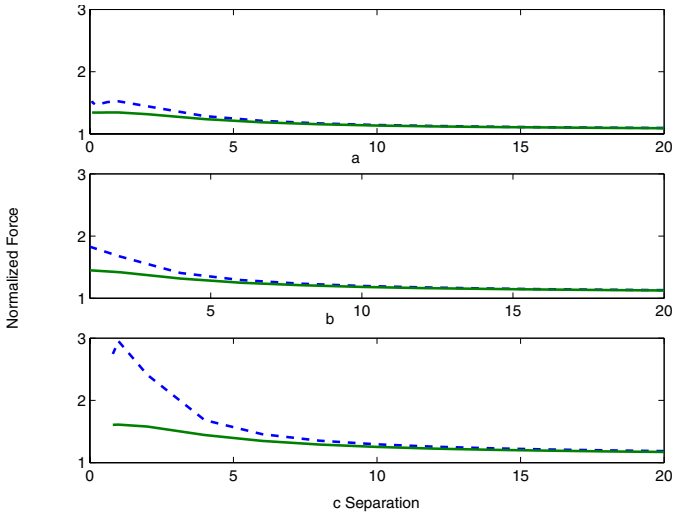

Fig. 13. Comparison of the analytical (—) and numerical (----) results for non-dimensional force versus separation for co-rotating tori (a) $\epsilon = 0.01$, (b) $\epsilon = 0.05$ and (c) $\epsilon = 0.25$.

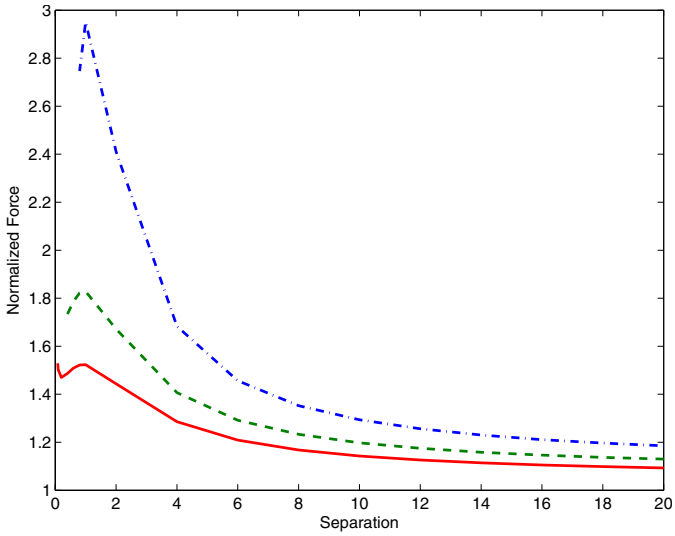

Fig. 14. Comparison of the numerical results for non-dimensional force versus separation for co-rotating tori in the lubrication limit (— $\epsilon = 0.01$, ---- $\epsilon = 0.05$, — · — · $\epsilon = 0.25$).

swimmer would have substantial shear, rotational and extensional components. Certain configurations can therefore lead to instabilities, setting the tori into rolling (if the tori lie in the same plane and their axes of symmetry parallel) or tumbling dynamics (if their axes of symmetry are perpendicular to each other) as the case may be. However, for small deviations from axisymmetry, and regimes in which such instability is not set in (small deviation of the axes of symmetry of the two tori), one may safely assume that there can be orientational order on account of the relative motion, leading ultimately to an axisymmetric configuration which is considered in the present case. These instabilities are known in vesicles and in biological systems like locomotion of ecoli [21,25,26].

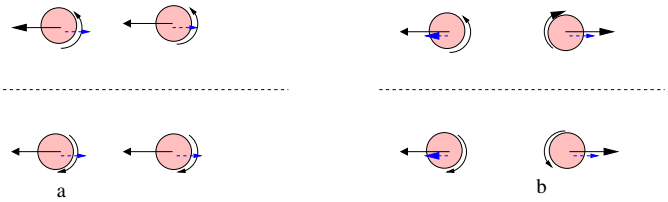

Fig. 15. Schematics of reinforcement and annihilation of forces in the co and counter rotating cases: solid arrow is for the single torus velocity while the dashed arrow indicates correction.

6 Conclusions

The hitherto unaddressed problem of interaction between two rotating tori is considered. These are best prototypes for self propelled particles and the interaction is important in understanding processes like bio-convection in such systems. The analysis is carried out for the case of co and counter-rotating tori. Two different instances are considered. Firstly, the interaction between two force-free tori is examined. For the co-rotating case the analysis indicates a strongly interacting regime with sharp reduction in the velocity indicating plausible attraction. In counter-rotation, the velocity tends to zero at a separation, which is dependent on the slenderness ratio. This raises the possibility of driven-assembly patterns in ensembles of such animals. The second problem investigated here, is estimation of the forces exerted on co and counter-rotating tori which do not translate. It is found that the force increases with separation for the case of co-rotating tori whereas for counter-rotation, the force decreases with distance. These results should be useful to study bio-convection patterns in a collection of rotating animals, and estimates of the shear stress exerted on such animals. The study should also prove useful in the hydrodynamic interaction between polymer molecules in a concentrated solution of miniplasmids or other stiff and semi-flexible polymers and in toroidal mixers in microfluidic devices.

The author thanks Igor Kulic and Helmut Schiessel for several useful discussions.

Appendix A: Elliptic Integrals

The complete elliptic integrals are defined as [27]:

$$F(k) = \int_0^{\pi/2} \frac{d\theta}{\sqrt{1 - k^2 \sin^2 \theta}} \tag{47}$$

$$E(k) = \int_0^{\pi/2} d\theta \sqrt{1 - k^2 \sin^2 \theta}. \tag{48}$$

The elliptic integrals have the following asymptotic expansion around $k = 1$,

$$F(k) = \frac{1}{2} \ln \left(\frac{16}{1 - k^2} \right) \tag{49}$$

$$E(k) = 1 + \frac{1 - k^2}{2} \left(\ln \frac{16}{1 - k^2} - \frac{1}{2} \right) \tag{50}$$

and around $k = 0$, the asymptotic expression reads

$$F(k) = \frac{\pi}{2} + \frac{\pi}{8}\, k^2 + \frac{9\pi k^4}{128} \tag{51}$$

$$E(k) = \frac{\pi}{2} - \frac{\pi}{8}\, k^2 - \frac{3\pi k^4}{128}. \tag{52}$$

$$I_1 = \int_0^{2\pi} \frac{d\theta}{\sqrt{1 - k\cos^2\theta/2}} = 4F(k)$$

$$I_2 = \int_0^{2\pi} \frac{\cos\theta}{\sqrt{1 - k\cos^2\theta/2}} d\theta = \frac{4}{k}\left((2-k)F(k) - 2E(k)\right)$$

$$I_3 = \int_0^{2\pi} \frac{d\theta}{\sqrt[3]{1 - k\cos^2\theta/2}} = \frac{4}{1-k}E(k)$$

$$I_4 = \int_0^{2\pi} \frac{\cos\theta}{\sqrt[3]{1 - k\cos^2\theta/2}} d\theta = \frac{4}{k}\left(\frac{2-k}{1-k}E(k) - 2F(k)\right)$$

$$I_5 = \int_0^{2\pi} \frac{\cos^2\theta}{\sqrt[3]{1 - k\cos^2\theta/2}} d\theta$$

$$= \frac{4}{k^2}\left(\frac{k^2 - 8k + 8}{1-k}E(k) - 4(2-k)F(k)\right)$$

$$I_6 = \int_0^{2\pi} \frac{d\theta}{\sqrt[5]{1 - k\cos^2\theta/2}}$$

$$= \frac{4}{3(1-k)}\left(\frac{2}{1-k}(2-k)E(k) - F(k)\right)$$

$$I_7 = \int_0^{2\pi} \frac{\cos\theta}{\sqrt[5]{1 - k\cos^2\theta/2}} d\theta$$

$$= \frac{4}{3k(1-k)}\left(\frac{2}{1-k}(1-k+k^2)E(k) - (2-k)F(k)\right)$$

$$I_8 = \int_0^{2\pi} \frac{\cos^2\theta}{\sqrt[5]{1 - k\cos^2\theta/2}} d\theta = \frac{4}{3k^2(1-k)}$$

$$\times \left((8 - 8k - k^2)F(k) - \frac{2(2-k)(2-2k-k^2)}{1-k}E(k)\right)$$

$$I_9 = \int_0^{2\pi} \frac{\cos^3\theta}{\sqrt[5]{1 - k\cos^2\theta/2}} d\theta$$

$$= \frac{4}{3k^3(1-k)}\left(\frac{2}{2-k}(k^4 + k^3 - 33k^2 + 64k - 32)E(k)\right)$$

$$+ \frac{4}{3k^3(1-k)}\left(-(2-k)(k^2 + 32k - 32)F(k)\right).$$

Appendix B: Calculations for a single torus

Velocity of a force free rotating torus

The velocity of a force free torus is obtained by substituting $f_{xo} = 0$ in equations (25) and (26). The strength of the dipole can be obtained from equation 26 as $d_{pxo} = -\frac{1}{8}$. Equation (25) indicates that the x velocity is given by

$$U_x = \frac{\epsilon^2}{2}\left(\log\frac{8}{\epsilon} - \frac{1}{2}\right). \tag{53}$$

This is the nondimensional translational velocity of a freely rotating torus. The dimensional velocity of a rotating torus with an angular velocity ω can therefore be given by

$$\tilde{U}_x = \frac{\omega b^2}{2a}\left(\log\frac{8a}{b} - \frac{1}{2}\right). \tag{54}$$

Calculation of force on a non-translating torus

To calculate the velocity field due to a rotating torus, prevented from translating by an external force, consider equations (25) and (26). Here $m_o = \frac{1}{2}$ satisfies the $O(\epsilon)$ equation. At $O(\epsilon^2)$, the quantities dependent on the angular parts can be balanced appropriately by $d_{pxo} = \frac{2f_{xo} - m_o}{4}$. The Stokeslet strength f_{xo} can be calculated by equating the translational velocity to zero, and the strength of the Stokeslet can now be easily determined as

$$f_x = -\frac{\epsilon^2}{4}\left[\frac{\ln(8/\epsilon) - 1/2}{\ln(8/\epsilon) + 1/2}\right]. \tag{55}$$

The strength of the potential dipole is then given by

$$d_{pxo} = -\frac{1}{4}\frac{\log\frac{8}{\epsilon}}{\log\frac{8}{\epsilon} + \frac{1}{2}}. \tag{56}$$

The local stress tensor can be expressed as $\mathbf{T} = [(\sigma_{xx}, \sigma_{xr}), (\sigma_{rx}\sigma_{rr})]$, where different elements of the stress tensor have following definitions:

$$\sigma_{xx} = -p + 2\frac{du_x}{dx} \tag{57}$$

$$\sigma_{xr} = \sigma_{rx} = \frac{du_x}{dr} + \frac{du_r}{dx} \tag{58}$$

$$\sigma_{rr} = -p + 2\frac{du_r}{dr}. \tag{59}$$

The traction vector (force per unit area) is $\mathbf{t} = \mathbf{T}\cdot\mathbf{n}$, and its value in the x direction is given by $\mathbf{e_x}\cdot\mathbf{T}\cdot\mathbf{n}$, where $\mathbf{n}$ is the unit normal given by $(\cos\psi, \sin\psi)$. The net force on the torus is then calculated by integrating the traction over the area of the torus given by $\int d\psi(1 + \epsilon\sin\psi)2\pi\,\epsilon$. Thus the net x directional non-dimensional force is given by

$$F_x = \int_0^{2\pi} d\psi(1 + \epsilon\sin\psi)2\pi\,\epsilon t_x = 4\pi^2\,\epsilon^2\frac{\ln(8/\epsilon) - 1/2}{\ln(8/\epsilon) + 1/2} \tag{60}$$

and the dimensional force by

$$\tilde{F}_x = 4\pi^2\mu b^2\frac{\ln(8/\epsilon) - 1/2}{\ln(8/\epsilon) + 1/2}. \tag{61}$$

Appendix C: Derivation of boundary integral equation

The basic equation for velocity at a point in flow over a particle, when the point lies outside the particle is given by

$$u_i(\mathbf{x}_0) = -\frac{1}{8\pi\mu}\int dS(\mathbf{x}) G_{ij}(\mathbf{x},\mathbf{x}_0) f_j(\mathbf{x}) + \frac{1}{8\pi}\int dS(\mathbf{x}) u_j(\mathbf{x}) T_{ijk}(\mathbf{x},\mathbf{x}_0) n_k(\mathbf{x}). \quad (62)$$

The first integral is called as single layer potential, whereas the second is called the double layer potential. When the singular point is moved on to the surface, the equation is modified as

$$u_i(\mathbf{x}_0) = -\frac{1}{4\pi\mu}\int dS(\mathbf{x}) G_{ij}(\mathbf{x},\mathbf{x}_0) f_j(\mathbf{x}) + \frac{1}{4\pi}\int dS(\mathbf{x}) u_j(\mathbf{x}) T_{ijk}(\mathbf{x},\mathbf{x}_0) n_k(\mathbf{x}). \quad (63)$$

The singularity in the double layer potential can be eliminated by re-writing the equation as

$$u_i(\mathbf{x}_0) = -\frac{1}{4\pi\mu}\int dS(\mathbf{x}) G_{ij}(\mathbf{x},\mathbf{x}_0) f_j(\mathbf{x}) + \frac{1}{4\pi}\int dS(\mathbf{x})(u_j(\mathbf{x}) - u_j(\mathbf{x_0})) T_{ijk}(\mathbf{x},\mathbf{x}_0) n_k(\mathbf{x}) + u_j(\mathbf{x_0})\frac{1}{4\pi}\int dS(\mathbf{x}) T_{ijk}(\mathbf{x},\mathbf{x}_0) n_k(\mathbf{x}). \quad (64)$$

Using the property of double layer potential,

$$\int dS(\mathbf{x}) T_{ijk}(\mathbf{x},\mathbf{x}_0) n_k(\mathbf{x}) = -4\pi\delta_{ij} \quad (65)$$

the governing equation can be re-written as

$$u_i(\mathbf{x}_0) = -\frac{1}{8\pi\mu}\int dS(\mathbf{x}) G_{ij}(\mathbf{x},\mathbf{x}_0) f_j(\mathbf{x}) + \frac{1}{8\pi}\int dS(\mathbf{x})(u_j(\mathbf{x}) - u_j(\mathbf{x_0})) T_{ijk}(\mathbf{x},\mathbf{x}_0) n_k(\mathbf{x}). \quad (66)$$

In the present work, it was found that the contribution of the second integral increases as the slenderness ration ϵ increases. This is understandable as the assumption of rigid body approximation becomes more invalid with ϵ. However, the absolute contribution of the second integral was found to be minimal and results were affected by around 1% (if the second integral was neglected) even in the case of a torus of thickness $\epsilon = 0.8$. The change was less than 0.1% for slender tori ($\epsilon < 0.05$)

References

1. G.I. Taylor, Proc. Roy. Soc. Lond., Ser. A **209**, 447 (1951)
2. J. Lighthill, Commun. Pure Appl. Math. **5**, 109 (1952)
3. E.M. Purcell, Amer. J. Phys. **45**, 3 (1977)
4. J. Avron, O. Gat, O. Kenneth, Phys. Rev. Lett. **93**, 186001 (2004)
5. N. Ali, R. Golestanian, J. Phys.: Condens. Matter **17**, S1203 (2005)
6. R. Dreyfus, J. Baudry, M. Roper, M. Fermigier, H. Stone, J. Bibette, Nature **6**, 862 (2005)
7. I. Kulic, R. Thaokar, H. Schiessel, Europhys. Lett. **72**, 527 (2005)
8. I.M. Kulic, R. Thaokar, H. Schiessel, J. Phys.: Condens. Matter **17**, S3965 (2005)
9. R.M. Thaokar, H. Schiessel, I.M. Kulic, EPJB p. Accepted (2007)
10. A.T. Chwang, W.S. Hwang, Physics of Fluids **2**, 1309 (1990)
11. N.A. Hill, T.J. Pedley, Fluid Dynamics Research **37**, 1 (2005)
12. I.M. Janosi, T. Tel, D.E. Wolf, J. Gallas, Phys. Rev. E **56**, 2858 (1997)
13. Y. Huang, N. Schorghofer, E. Ching, Europhys. Lett. **52**, 399 (2000)
14. G. Taylor, Proc. Roy. Soc. Lond., Ser. A. **211**, 225 (1952)
15. E. Guyon, J. Hulin, L. Petit, C. Mitescu, *Physical hydrodynamics* (Oxford University Press, Oxford, 2001)
16. D. Guell, H. Brenner, R. Frankel, H. Hartman, J. Theor. Biol **135**, 525 (1988)
17. M. Ramia, N. Phan-Thein, Biophysical J **65**, 755 (1993)
18. R. Nasseri, N. Phan-Thein, Comput. Mech. **20**, 551 (1997)
19. J. Lega, T. Passot, Nonlinearity **20**, C1 (2007)
20. H. Jiang, T.R. Osborn, C. Meneveau, J. Plank. Res **24**, 235 (24)
21. T. Ishikawa, M. Simmonds, T. Pedley, J. Fluid Mech. **568**, 119 (2006)
22. C. Pozrikidis, *Boundary integral and singularity methods for linearized viscous flow* (Cambridge University Press, Cambridge, 1992)
23. S. Kim, S. Kariala, *Microhydrodynamics* (Butterworth-Heinemann, MA, USA, 1991)
24. G.K. Youngren, A. Acrivos, J. Fluid Mech. **6**, 377 (1975)
25. S. Sukumaran, U. Seifer, Phys. Rev. E. **64**, 011916 (2001)
26. J. Alder, W.W. Tso, Science **184**, 1292 (1974)
27. M. Abramowitz, I. Stegun, *Handbook of mathematical functions* (Dover, New York, 1964)